Research Article | Vol. 26, No. 12 | 11 Jun 2018 | OPTICS EXPRESS 14999
Optics EXPRESS

Interferometric analysis of sub-nanosecond laser-induced optical breakdown dynamics in the bulk of fused-silica glass

V. H. NGUYEN,[1] M. KALAL,[2] H. SUK,[1,4] AND K. A. JANULEWICZ[1,3,5]

[1]*Department of Physics and Photon Science, Gwangju Institute of Science and Technology, 123 Cheomdangwagi-ro, Buk-gu, Gwangju, 61005 South Korea*
[2]*Faculty of Nuclear Sciences and Physical Engineering, Czech Technical University in Prague, Brehova 7, 115 19 Prague 1, Czech Republic*
[3]*Currently with the the Institute of Optoelectronics of the Military University of Technology, 2 Kaliski Str., 00-908 Warsaw, Poland*
[4]*hysuk@gist.ac.kr*
[5]*karol.janulewicz@wat.edu.pl*

Abstract: Dynamics of laser-induced optical breakdown in the bulk of fused-silica glass irradiated by a sub-nanosecond laser pulse at a wavelength of 790 nm with a fluence of 522 J/cm^2 was studied by the femtosecond time-resolved complex interferometry in Nomarski arrangement utilising a Fresnel bi-prism. Evolution of the plasma channel and the development of the free electron density were in focus of the investigation. The measured ultimate length of the plasma channel was equal to 30 μm and almost doubled the length estimated within the moving breakdown model. The history of the transient electron density distribution in the plasma was reconstructed from the phase shift maps using the inverse Abel transform and it revealed further deviation from this model. The core of the plasma channel exhibited at the last stages of the development a considerable level of the electron density up to 2.4×10^{20} cm^{-3}. The signature of the pre-breakdown phase has been identified as radiation caused by ionization-released electrons interacting with ions and has been demonstrated in solids for the first time in this way. Origin of the discrepancy between the theoretical prediction of the moving breakdown model and the measured values of the channel length is discussed as well.

OCIS codes: (140.3440) Laser-induced breakdown; (140.3330) Laser damage; (100.0118) Imaging ultrafast phenomena; (180.0180) Interferometry; (350.7420) Plasma electron density.

References and links

1. C. B. Schaffer, A. Brodeur, and E. Mazur, "Laser-induced breakdown and damage in bulk transparent materials induced by tightly-focused femtosecond laser pulses," Meas. Sci. Technol. **12**, 1784 (2001).
2. B. C. Stuart, M. D. Feit, S. Herman, A. M. Rubenchik, B. W. Shore, and M. D. Perry, "Nanosecond-to-femtosecond laser-induced breakdown in dielectrics," Phys. Rev. B **53**, 1749 (1996).
3. C. W. Carr, J. D. Bude, P. DeMange,"Laser-supported solid-state absorption fronts in silica," Phys. Rev. B **82**, 184304 (2010).
4. Y. Hayasaki, M. Isaka, A. Takita, and S. Juodkazis, "Time-resolved interferometry of femtosecond-laser-induced processes under tight focusing and close-to-optical breakdown inside borosilicate glass," Opt. Express **19**, 5725 (2011).
5. Y. Hayasaki, M. Isaka, A. Takita, and S. Juodkazis, "Time-resolved axial-view of the dielectric breakdown under tight focusing in glass," Opt. Mat. Express **1**, 1399 (2011).
6. K. A. Tran, Y. V. Grigorov, V. H. Nguyen, Z. U. Rehman, N. T. Le, and K. A. Janulewicz, "Time-resolved shadowgraphy of optical breakdown in fused silica," Proc. SPIE **9532**, 953205 (2015).
7. A. A. Manenkov, "Fundamental mechanisms of laser-induced damage in optical materials: today's state of understanding and problems," Opt. Eng. **53**, 010901 (2014)
8. P. H. Rose, "Recent experiments in laser supported absorption waves," Acta Astronaut. **2**, 941 (1975).
9. E. N. Glezer, E. Mazur, "Ultrafast-laser driven micro-explosions in transparent materials," Appl. Phys. Lett. **71**, 882–884 (1997).
10. M. Kalal, M. Krupka, J. Dostal, R. Dudzak, J. Ullschmied, "Complex interferometry principles and its potential in case of reference interferograms availability, " in Proceeding of the First European Physical Society Conference on

#324969 https://doi.org/10.1364/OE.26.014999
Journal © 2018 Received 27 Feb 2018; revised 4 May 2018; accepted 5 May 2018; published 30 May 2018

Optics EXPRESS

Plasma Diagnostics, ed. (Proceedings of Science 2015) 014.
11. Yu. B. Raizer, "Breakdown and heating of gases under the influence of a laser beam," Sov. Phys. Usp., **8**, 650–673 (1966).
12. F. Docchio, P. Regondi, M. R. C. Capon, and J. Mellerio, "Study of the temporal and spatial dynamics of plasmas induced in liquids by nanosecond Nd:YAG laser pulses. 1: Analysis of the plasma starting times," Appl. Opt. **27**, 3661 (1987).
13. C. Shen, M. Chamboneau, X. Cheng, Z. Xu, and T. Jiang, "Identification of the formation phases of filamentary damage induced by nanosecond laser pulses in bulk fused silica," Appl. Phys. Lett. **107**, 111101 (2015).
14. A. Smith, B. Do, M. Soderlund, "Deterministic Nanosecond Laser-Induced Breakdown Thresholds In Pure and Yb3+ Doped Fused Silica," Proc. of SPIE Fiber Lasers IV: Technology, Systems, and Application **6453**, 645317 (2007).
15. R. Root, A. Pirri, "Long-time laser induced breakdown of particulate contaminated air," AIAA, Aerospace Sciences Meeting, 17th, New Orleans, La., Jan. 15-17, 1979, p. 16.
16. S. Juodkazis, K. Nishimura, S. Tanaka, H. Misawa, E. G. Gamaly, B. Luther-Davies, L. Hallo, P. Nicolai, and V. T. Tikhonchuk, "Laser-induced microexplosion confined in the bulk of a sapphire crystal: Evidence of multimegabar pressures," Phys. Rev. Lett. **96**, 166101 (2006).
17. A. Vogel, K. Nahen, D. Theisen, and J. Noack, "Plasma formation in water by picosecond and nanosecond Nd: YAG laser pulses. I. Optical breakdown at threshold and superthreshold irradiance," IEEE J. Sel. Top. Quantum Electron. **2**, 847–859 (1996).
18. M. Takeda, H. Ina, and S. Kobayashi, "Fourier-transform method of fringe-pattern analysis for computer-based topography and interferometry," J. Opt. Soc. Am. **72**, 156 (1982).
19. M. Kalal and K. A. Nugent, "Abel inversion using fast Fourier transforms," Appl. Opt. **27**, 1956–1959 (1988).

1. Introduction

Laser-induced optical breakdown in transparent dielectrics remains an active research area for a long time. In the beginning, glasses and crystals were the main objects of interest mainly due to their importance for the development of high power laser systems. The increasing importance of the laser material processing or more generally, the material sciences, shifted the focus of interest in the laser-induced breakdown research towards the fundamentals of the effect and to its potential as a source of the extreme thermodynamics conditions. Recent studies of the laser-induced breakdown in dielectrics have paid strong attention to the physics of the optical breakdown, plasma formation, absorption mechanisms and some hydrodynamic effects (shocks) [1–6].

There exist still differences in interpreting some of the fundamental breakdown parameters. One of the controversies regards the laser-induced breakdown threshold (LIBT). For the sake of clarity, LIBT should be distinguished from the laser-induced damage threshold (LIDT). It has been pointed out in [7] that the quite arbitrary definition of LIBT (the moment when n_e=n_{cr}) has no real reference to the physics, and as a consequence, knowledge of the electron production dynamics during the process is of fundamental importance. Rate of the electron density variation decides about the breakdown character, i.e. it can be either a relatively smooth, resembling laser-supported combustion (LSC) [8] or to be a very brute force of laser microexplosion comparable to the laser-supported detonation (LSD) [8, 9]. The need for more precise diagnostic tools of a high temporal resolution arises with the increasing deposition rate of the driving energy.

During the optical breakdown a very high density of free electrons of the order of 10^{18}-10^{20} cm^{-3} used to be generated in the ionization process. The common diagnostic techniques employed to determine the electron density include Langmuir probe, Thomson scattering or the most powerful of them - the laser interferometry. Interferometry is a very appealing method for accurate determination of the plasma density, especially for studying axially symmetric, small-scale plasmas (a few microns in diameter) and early phases of the plasma density development. The most common configurations for the density measurements of laser-induced plasmas are those developed by Michelson, Mach-Zehnder and Nomarski. The Michelson-type interferometer was used in [4, 5] to study with very high temporal resolution the breakdown initiated by a tightly focused femtosecond laser pulse in a glass. Recent report [10] suggested employing complex interferometry with reference interferograms, enabling determination not only the usual phase shifts, but also simultaneous reconstruction of the probe beam amplitude. The use of the Michelson-type interferometer has, in our opinion, limitation as the probe beam passes through

Optics EXPRESS

the plasma medium twice, thereby complicating alignment, data reduction and reducing the experiment resolution. In contrast, the Nomarski interferometer utilizing a Fresnel bi-prism is relatively simple, easy to align, flexible in arrangement and very stable.

Plasma evolution of the breakdown process driven by nanosecond and sub-nanosecond pulses used to be interpreted within the classical model of the moving breakdown formulated by Raizer [11] and later upgraded by Docchio *et al.* [12]. The model includes some simplifying assumptions as negligibility of the time required for the breakdown beginning, independence of the breakdown threshold of the beam diameter and constancy of the threshold in time, i.e. plasma formed early during the laser pulse does not influence the breakdown threshold in its vicinity. These assumptions were formulated to build the relation between the maximum plasma length z_{max} and the laser pulse energy normalized to the threshold value [12]. Recently, there appeared reports on overestimated length of a plasma channel obtained within the moving breakdown model [13].

In the work presented in this paper, dynamics of the laser-induced optical breakdown in the bulk of fused-silica glass initiated by a tightly focused sub-nanosecond (≃300 ps) laser pulse was investigated with the pump-probe technique utilising femtosecond Nomarski complex interferometer equipped with a Fresnel bi-prism. The full history of formation and expansion of the laser-induced plasma channel was extracted from the interferograms by the probing beam amplitude reconstruction. The experimental data was confronted with the prediction of the moving breakdown model and the latter seems to underestimate length of the created plasma channel at a very high driving power. Our explanation makes very fast laser-supported absorption responsible for that. The spatio-temporally resolved complex interferometric technique was also used to determine quantitatively dynamics of the of the plasma density in the laser-induced plasma.

2. Experimental detail

A setup of the Nomarski interferometer based on a Fresnel bi-prism within the experimental pump-probe arrangement is shown in Fig. 1. The driving laser pulse (FWHM equal to 314 ps, measured by a fast photodiode connected to a Teledyne LeCroy WaveMaster 816Zi 16 GHz oscilloscope) was out-coupled behind the front-end of the main femtosecond Ti:sapphire laser system working at 790 nm. The pump pulse was focused inside the fused-silica glass by a 20X–microscope objective (MO) with a numerical aperture NA of 0.4. The focal plane was located approximately 500 μm below the sample surface. The $1/e^2$-diameter of the focused pump pulse was experimentally estimated (at very low irradiation energy) to be equal to 2.66 μm. The probe laser pulse, generated by out-coupling a small part of the laser energy from the compressed pulse of the main laser system. It operated at the second harmonic, i.e. at a wavelength of 395 nm, and had a length of ~50 fs (FWHM) at the sample. This pulse was used to register development of the optical breakdown by traversing the created plasma in the direction perpendicular to the axis of the pump beam.

A low-resolution optical delay line denoted in Fig. 1 as ODL1 was placed in the pump beam pathway in order to variate in a broad range the time interval between the pump and probe pulses arriving to the interaction area. An additional, more accurate optical delay line ODL2 was located in the probe beam pathway to obtain a femtosecond temporal resolution of the observation. The interference fringes generated by the breakdown area were imaged on the sensor of a 16-bit Andor CCD (Neo sCMOS) camera by an optical system including a zoom lens. A set of two bandpass filters (BPFs) with a bandwidth of 40 nm centred at 400 nm was employed to prevent the residual radiation of the fundamental frequency and significant part of the plasma emission from entering the CCD. Although duration of the probe pulse was shortened after the second harmonic generation in a BBO crystal, the effective duration of the diagnostic pulse was about 45-50 fs, slightly elongated due to presence of optical elements in the probe beam. The sample

Optics EXPRESS

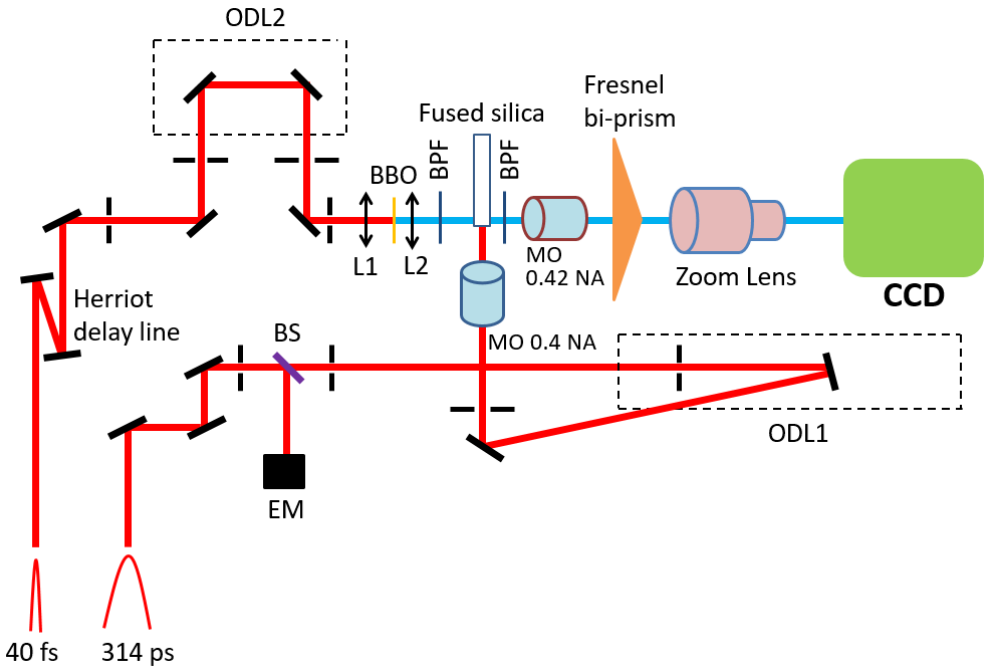

Fig. 1. The setup of the Nomarski interferometer based on a Fresnel bi-prism dedicated to the time-resolved diagnostic in a pump-probe arrangement; L: lens, MO: microscope objective, BS: beam splitter, BPF: bandpass filter, NA: numerical aperture, EM: energy meter.

was moved by a motorized XYZ translational stage to ensure a fresh material for each shot. Due to the limited length of ODL2 the maximum time delay under a high precision resolution was limited to 1.023 ns. Longer delay times (> 1.023 ns) were achieved by manual adjustment of an auxiliary path elongation system (ODL1). This system utilised two large-aperture mirrors in the multiple-reflection arrangement to vary the length of the probe beam path. The magnification of the images was kept constant during the whole experiment to control spatial scaling and quantitative estimates of the dimensions. All optical components in the set-up were precisely re-aligned with a He-Ne laser after each change of irradiation conditions.

The measurement of the pump pulse duration helped to interpret the interaction process more accurately. Pump pulse duration at a level of $1/e^4$ of I_{max} was estimated to be 754 ± 5 ps. The pulse reproduced a temporal Gaussian shape with a very good accuracy. Energy of the driving pulse focused onto the samples was 29 ± 0.1 μJ and remained unchanged during the whole experiment. The delay times were defined in relation to the peak of the pump laser pulse chosen as "0".

3. Results and discussions

Example interferograms of the laser-induced breakdown in the bulk of fused-silica glass generated by a 314-ps laser pulse (FWHM) with a fluence of 522 J/cm^2 are shown in Fig. 2. They cover the development between the time delays of -204 ps and 12.796 ns and are presented with a white dashed-line marking the approximate geometrical focal plane of the pump pulse. This feature is present in all images of the channel. The breakdown threshold energy was determined here as the pulse energy giving the first visible deformation of the interferogram and was equal to ≃9 μJ. This value corresponds to the threshold intensity of 5×10^{11} W/cm^2. Interestingly, Smith *et al.*

Optics EXPRESS

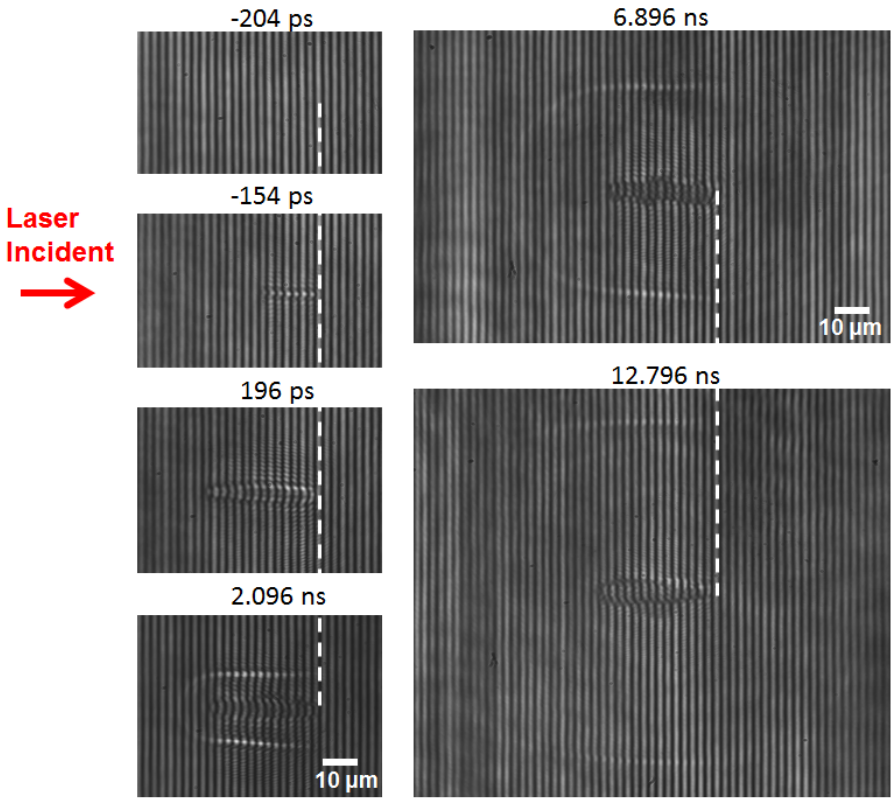

Fig. 2. Interferograms recorded at different moments of the laser-induced breakdown generated by a 314-ps laser pulse (FWHM) in the bulk of fused-silica glass with a fluence of 522 J/cm^2; the images cover the development between a time delay of -204 ps and 12.796 ns; the white dashed-line is for alignment of plasma channel length.

reported in [14] the same value of the threshold intensity at a wavelength of 1064 nm with a pulse length of 7.5 ns. Hence, our approximate estimate method seemed to work reasonably. The first visible changes caused by the breakdown were observed directly after a time delay of t_0 = -204 ps, i.e. long before the peak of the pump pulse (taken as the "0" delay point). The images were recorded in the 500 fs steps. The plasma channel length has grown up to ≃30 μm in average, and the growth was completed at a time delay of 196 ps, i.e. well after the pulse peak and in contrast to the commonly accepted conclusion of the breakdown moving mirror model.

The sequence of images presented in Fig. 3 shows distributions of the probe pulse amplitude, extracted from the interferograms at different time delays between -204 ps and 12.796 ns. Surprisingly, a signal trace in the probe pathway was visible over the full length of the channel already at a delay of -204 ps, when it should be absent. Lack of any visible deformation of the interference fringes at this delay suggests that the phase changes were below sensitivity of the system and hence negligible. In other words, thermal changes of the lattice stability or modification of the refraction index could be ignored. It is very likely that the low-level part of the incident laser pulse (below the bulk breakdown threshold) interacted primarily with bound electrons of the material electronic system, released them, and these free electrons of low density excited the ions or were decelerated in the ionic structure, in both cases emitting radiation. This radiation was retrieved from the probe signal after using the reference interferogram in the complex interferometry. Analogous effect of the luminous pre-breakdown phase was observed in gases

Optics EXPRESS

and denoted as the laser-induced spark light (lighting right before the optical breakdown) [15]. The transition moment from the spark light to the breakdown phase is perfectly seen in Fig. 3 by comparing the images of the probe amplitudes for the time delays of -204 ps and -202 ps. A yellow vertical arrow in the image at -202 ps indicates the border between the plasma channel (dark area due to high electron density) and the bright spark light. This is the first such a direct proof of the pre-breakdown phenomena in solids. Once the breakdown threshold was exceeded, a high density of free electrons was achieved dominantly by the electron avalanche process. Non-linear radiation absorption and intense lattice heating followed the breakdown and resulted in the irreversible structural transformations leading to the damage inside the bulk [3, 13, 16].

Importantly, the longest laser-induced spark light (in our experiment ≃30 μm) quite well reproduced the ultimate laser-induced plasma channel length at 196 ps. It allows for prediction of the final plasma channel length in a given focusing geometry already at intensities below the damage threshold. The sequence of images in Fig. 3 confirmed also some of the basic assumptions of the moving breakdown model. The probe amplitude distribution reconstructed from the recorded interferograms revealed that the channel end was broadened at the late phase of the breakdown development (here about 12.796 ns) and this corresponds well with the observation in [13]. The shock wave expansion, the rarefaction wave and the thermal effect were mainly responsible for the broadening [13].

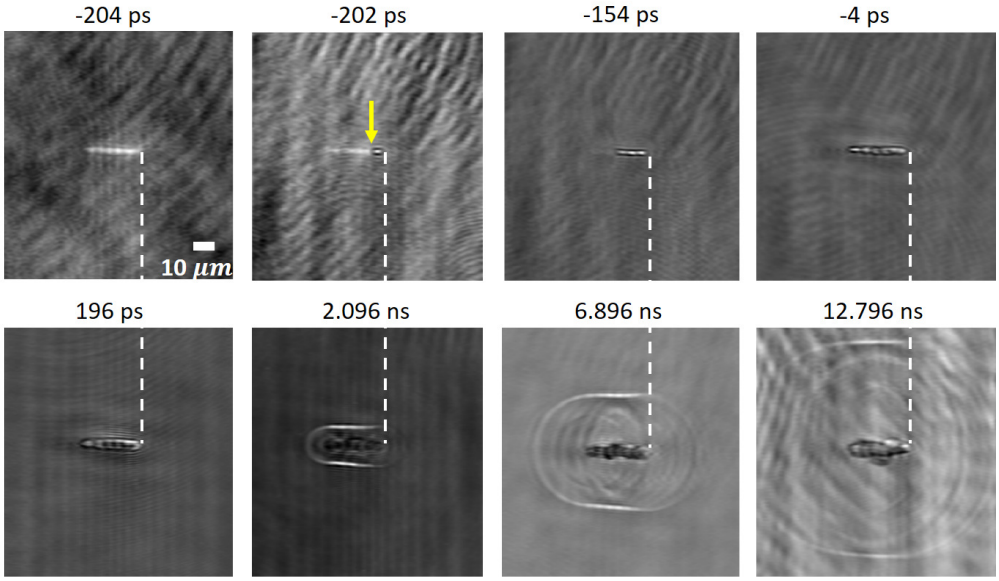

Fig. 3. Images of the probe amplitude distribution extracted from the interferograms; channel formation between the time delays of -204 ps and 12.796 ns is covered; the white vertical dashed line is for alignment of plasma channel length; the yellow vertical arrow shows the border between the plasma channel and the spark light.

The plot presented in Fig. 4 illustrates development of plasma channel length as a function of the time delay in relation to the temporal profile of the pump pulse. The plasma channel grew rapidly in the axial direction within the first 200 ps, achieving a length of 28.4 μm (nearly the final length) at the time delay of -4 ps. This time interval defines the dominant part of the growth, ending slightly before the pump laser pulse peak. However, achieving the final length of ≃30 μm needed additional 200 ps (up to the delay of +196 ps). During the last quarter of the laser pulse length, i.e. for 181 ps, the laser pulse did not deliver enough energy to elongate further

Optics EXPRESS

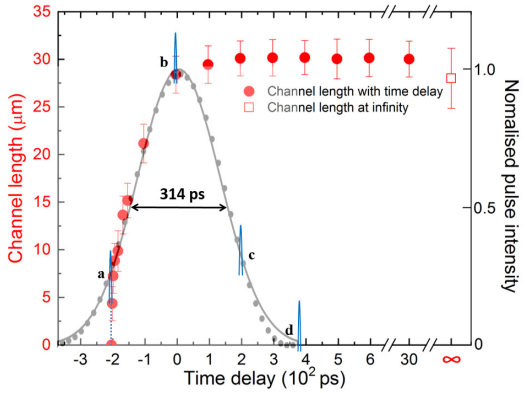

Fig. 4. Development of the channel length in time (measured as a function of the delay time). Experimental temporal profile of the driving laser pulse (with FWHM equal to 314 ps) is fitted by the Gaussian function (the black solid line) and is normalized to the pulse intensity. The probe pulses are sketched in the blue-color and propagate from left to right. a) the breakdown threshold; b) the plasma channel with a length of (≃28.4 μm) is almost completed close to the peak of the pump pulse; c) completion of the plasma channel (length of ≃30 μm); d) situation at the end of the laser driving pulse.

the plasma channel. This was consistent with the assumption of the moving breakdown model that no interaction with the plasma occurs when the laser irradiance falls below the breakdown threshold [12, 17]. However, the model assumption of the interaction stop at the pulse peak was in disagreement with the observation. The ultimate length of the plasma channel, equal to ≃28 μm, has been reached after the cooling-induced shrinking (marked by the red square in Fig. 4). Moreover, the maximum extent of the breakdown region calculated within the model was no longer than 15.2 μm, and this merely halves (roughly) the experimental value. Looking for the reason of this dramatic discrepancy we paid more attention to the parameters used in our estimate process. The Rayleigh length of the focused beam might be, in reality, larger than the estimate of $z_R = (n\pi w_0^2)/\lambda = 10.22$ μm obtained for a wavelength of λ=790 nm and with the fused silica's refractive index equal to $n = 1.4535$ (the table value). A beam waist diameter measured in the air was equal to $2w_0$= 2.66 μm, while a measured diameter of the laser-induced spark was only marginally larger than that value and equal to ≃3 μm. Energies taken to determine the factor β= E_p/E_{th} were carefully measured and where equal to $E_m = 29$ μJ and $E_{th} = 9$ μJ. Taking into account the possible energy measurement errors, the inaccuracy of the predicted channel length $z_{max} = z_R \times \sqrt{\beta - 1}$ was within 10 percent. A value of parameter $A=\tau_p/2\sqrt{2ln2} = 133.36$, with $\tau_p = 314$ ps, was consistent with a value of this parameter calculated from the experimentally determined moment of the breakdown beginning ($t_0=-A\sqrt{2ln\beta} \simeq -204$ ps). Hence, correctness of our estimate seems to be fairly justified.

The discrepancy between the theoretical value of the channel length and that observed in our experiment could be caused by the model's simplifying assumptions of constancy both the breakdown threshold value and the absorbed energy as well as ignoring the plasma influence on the closest neighbourhood. In the presented experiment, the plasma formed during the early phase of the breakdown, especially due to very strong irradiation, could reach a disproportional increase in temperature and pressure stimulating the band gap collapse in the surrounding material and transforming it into an absorber. The thermal conduction would support forming a fast absorption front by decreasing effectively the breakdown threshold at other points upstream the laser beam [3]. Extremely fast movement of the absorption front registered in the experiment supports this scenario.

Optics EXPRESS

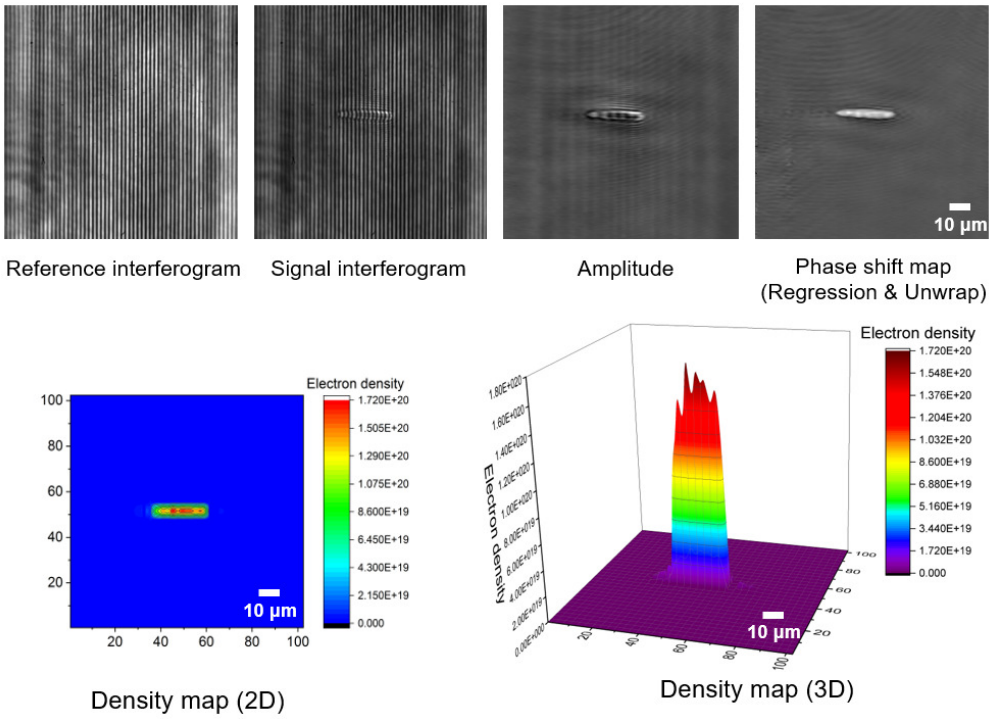

Fig. 5. The processed interferometric data for a time delay of 196 ps.

The essential aim of the interferometric experiment was determination of the transient electron density distribution during the development of the laser-induced breakdown. The exemplary interferograms presented in Fig. 5 were recorded at a delay of 196 ps (the moment when the plasma channel growth has been completed). The reconstruction procedure of the electron density map from the interferograms conducted for different time delays relied on determining the normalized visibility function V_{norm}=V_{sign}/V_{ref}. The respective functions V_{sign} and V_{ref} were obtained from the signal and reference (without pump laser pulse) interferograms, respectively, for each time delay. The visibility function allowed for determining the phase shifts. The maps of the amplitude and phase shift of the probe pulse at a given time delay have been created from the fringe patterns by applying Fourier transform with the central- and side-lobe selections, respectively. Possible discontinuities in the reconstruction have been removed by adding an offset phase [18]. The electron density maps (2D and 3D views) were extracted from the phase shift map by applying the inverse Abel transformation according to the procedure described in [19]. In the region of plasma channel, the electron density was of the order of 10^{20} cm^{-3}. The maximum electron density at a delay time of 196 ps reached 1.72×10^{20} cm^{-3}, a value well below the critical density for the probe beam. This confirmed the assumption of the moving breakdown model concerning distributed character of absorption. Interestingly, an electron density level of (4-5) $\times$ 10^{20} cm^{-3} generated with femtosecond pulses in borosilicate glass was reported in [5]. The same authors expressed in other paper a guess that directly before the breakdown transient (reversible) phase changes could occur [5]. Our earlier comments regarding the laser-induced spark light suggest that indeed, before beginning the cavitation under irradiation of sub-nanosecond pulses, there is a phase of lighting along the full length of the channel but without any noticeable distortion of the interference fringes. However, closer inspection of the plasma channel vicinity (see phase-shift map in Fig. 5) allows for revealing very weak changes of the probe phase. The

Optics EXPRESS

variation of the axial electron density distribution in the plasma channel from the early moment of the energy deposition (-202 ps) to the moment of the plasma channel growth completion (196 ps) is shown in Fig. 6(a).

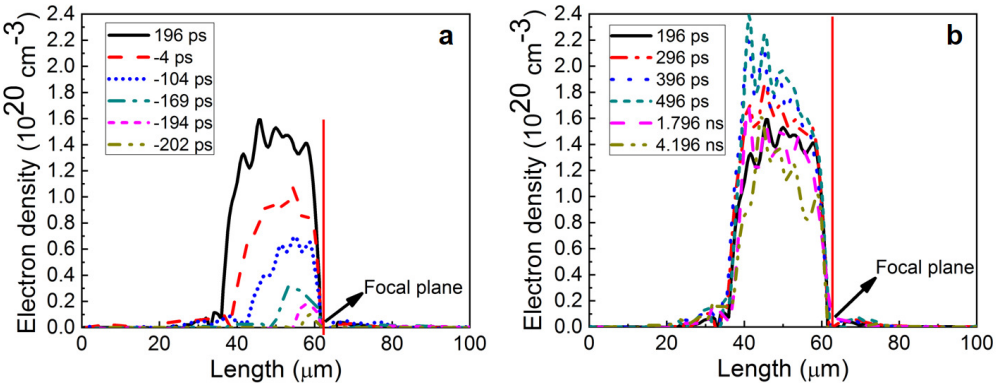

Fig. 6. Development in time of the axial electron density distribution in the plasma channel for: a) the time delays between -202 ps and 196 ps and b) the time delays between 196 ps and 4.196 ns.

At a time delay of -202 ps, the material has absorbed only a small amount of the pulse energy, generating free electrons of limited density but without significant change in the refraction index. The maximum electron density in the middle of the channel length was 1.01 $\times 10^{19}$ cm^{-3}, but it was increasing gradually with the elapsing time. The front of the free electrons moved in this process backward, i.e. towards the irradiation source, but there was no dominating maximum in the axial distribution. With the increase of the deposited laser energy, within the interval between -202 ps and -194 ps, additional free electrons were created to initiate the avalanche ionization process leading to a rapid growth of the free electrons population at a rate of 9.2 $\times 10^{17}$ cm^{-3}/ps, as shown in Fig. 7. Free electron density increased also due to effect of some electrons accelerated to energies higher than the band gap width. During the time interval between -194 ps and -104 ps, the ionization growth rate was about 6 $\times 10^{17}$ cm^{-3}/ps. During the late formation phase of the plasma channel (the time delays between -104 ps and +196 ps) the electron density increased at a constant rate equal to about 3.5 $\times 10^{17}$ cm^{-3}/ps. It is worth noting that the major part of the pump

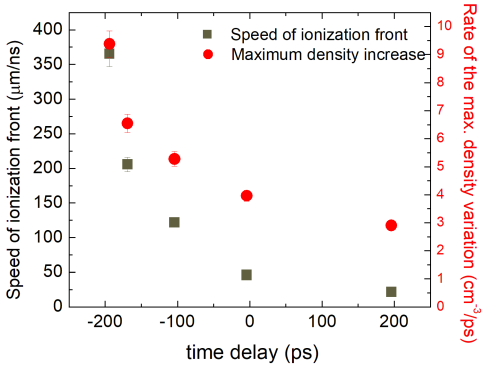

Fig. 7. The ionization front speed and the increase rate of the electron density maximum both vs.time delay.

Optics EXPRESS

energy pulse was deposited between the beginning of the pump pulse and the time delay of 196 ps. This yielded the high temperature and high pressure plasma with an electron density of 1.72 $\times 10^{20}$ cm^{-3}. After that, the plasma channel length remained constant at $\simeq 30$ μm. This was in some small part caused by the additional amount of the laser energy delivered between a time delay of 196 ps and the termination of the pulse at 377 ps but most likely it resulted from high temperature and the thermal effects finishing the process at 496 ps, as described in [3]. Later, at a time delay of 896 ps the electron density decreased to about 1.5×10^{20} cm^{-3} due to cooling down the plasma. This electron density did not varied much and remained nearly constant until 4.196 ns.

4. Conclusions

Summarising, the femtosecond temporally resolved complex interferometry of the sub-nanosecond laser-induced breakdown in the bulk of fused-silica glass has been presented with the goal to extend knowledge on dynamics of the breakdown process, especially on spatio-temporal development of the electron density. A well-tested numerical code based on the fast Fourier transform and the inverse Abel transform was used to extract images of the amplitude and phase of the probe signal as well as electron density distributions from the interferograms. Investigation of the plasma channel length growth under conditions of very strong irradiation revealed existence of the spark light in the pre-breakdown phase and it has been shown in this form for the first time for solids. The effect could be useful to predict the final channel length and to assert the primary energy deposition place by simple low-level, sub-threshold irradiation. Moreover, the classical model of moving breakdown failed to evaluate correctly the plasma channel length under our experimental conditions halving the values obtained in the experiment. We ascribed it to invalidity of the model simplified assumptions at the extreme irradiation conditions of our experiment. The development of the axial electron density distribution in the plasma channel from the beginning of the breakdown up to the time delays in the nanosecond range has been investigated in intrinsic relation with the growth of the plasma channel. The results deviated again slightly from the prediction or assumptions of the moving breakdown model.

Funding

Ministry of Education, Science and Technology of Korea through Basic Science Research Program (No.), by BK21+ project, Gwangju Institute of Science and Technology through the Top Brand Project (TBP).